OMI/AURA, SCIAMACHY/ENVISAT AND GOME2/METOPA SULPHUR DIOXIDE ESTIMATES; THE CASE OF EASTERN ASIA.

M. E. Koukouli[(1)], D. S. Balis[(1)], N. Theys[(2)], H. Brenot[(2)], J.van Gent[(2)], F. Hendrick[(2)], T. Wang[(3)], P. Valks[(4)], P. Hedelt[(4)], G. Lichtenberg[(4)], A. Richter[(5)], N. Krotkov[(6)], C. Li[(6,7)] and R. van der A[(8)]

(1) Laboratory of Atmospheric Physics, Aristotle University of Thessaloniki, Thessaloniki, Greece.

(2) Belgian Institute for Space Aeronomy, Brussels, Belgium.

(3) Institute of Atmospheric Physics, Chinese Academy of Sciences, Beijing, China.

(4) German Aerospace Center, Remote Sensing Technology Institute, Germany.

(5) Institute of Environmental Physics, University of Bremen, Bremen, Germany.

(6) NASA Goddard Space Flight Center, Greenbelt, MD, USA

(7) Earth System Science Interdisciplinary Center, College Park, MD, USA

(8) Koninklijk Nederlands Meteorologisch Instituut (KNMI), De Bilt, the Netherlands

ABSTRACT

The EU FP7 *Monitoring and Assessment of Regional air quality in China using space Observations, Project Of Long-term sino-european co-Operation*, MarcoPolo, project focuses on deriving emission estimates from space, http://www.marcopolo-panda.eu. Long term satellite observations of Sulphur Dioxide, SO_2, over the greater China area from the SCIAMACHY/Envisat, GOME2/MetopA and OMI/Aura missions are compared and their relative strong points and limitations are discussed. For each satellite instrument, two different datasets are being analyzed in the same manner. Rigorous spatiotemporal statistical analysis based on novel analysis techniques is performed for each data set in order to reduce noise and biases and enhance pollution signals in satellite datasets. Furthermore, identification of point sources such as power plants, smelters and urban agglomerations, as well as definition of their relative contribution to the regional SO_2 levels, form the main findings of this investigation. Trend analyses and their statistical representation help locate regions of interesting SO_2 loading in China.

1. INTRODUCTION

With the generalized usage of satellite observations as a means for air quality control and environmental assessment on a global scale, the focus of the scientific community has turned to monitoring developing countries. Since the anthropogenic pollution of the atmosphere is not a local phenomenon, but may affect neighboring states and even in some cases entire latitude belts [1;2], monitoring the state of the atmosphere from space has proved a very valuable tool. Sulfur dioxide (SO_2) is a short-lived gas which is primarily created by volcanoes, power plants, refineries, metal smelting and the burning of fossil fuel. This fossil fuel burning occurs near the surface where SO_2 is released into the planetary boundary layer (PBL). There, the mean lifetime varies between one and two days or even less, to up to more than a month in the stratosphere [e.g., 3].

The largest increases in tropospheric SO_2 emissions have occurred in Asia during the last 20 years [4]. Many recent studies have hence focused in that region, using satellite, aircraft, *in situ* as well as modeling inputs. In [5] the SO_2 over Central China was studied using measurements as well as numerical simulations and it was indicated that ~50% of the anthropogenic sulfur emissions were transported downwind, and that the overall lifetime of tropospheric SO_2 was 38 ± 7 h. The potential application of the OMI/Aura PBL SO_2 product to regional air pollution studies was shown in [6] in NE China, where the satellite observations were shown to qualitatively agree with the aircraft in situ observations of high SO_2 column amounts ahead of a cold front and lower concentrations behind it hence demonstrating that OMI can distinguish between background SO_2 conditions and heavy pollution on a daily basis. Satellite observations have also the capability of monitoring air pollution episodes at a regional scale and to track the transport and evolution of the plume on the following days, as was shown for pollution originating in China moving to the NW Pacific [7]. Similarly however, in recent years, signs of decrease over certain regions were shown by satellite observations in [8] among others. These reductions shown by the OMI/Aura datasets confirm the effectiveness of the flue-gas desulfurization devices in reducing SO_2 emissions, which likely became operational between 2007 and 2008.

Due to the strong economic growth in China in the past decade, air pollution has become a serious issue in many parts of the country. The EU FP7 *Monitoring and Assessment of Regional air quality in China using space Observations, Project Of Long-term sino-european co-*

Proc. 'ATMOS 2015, Advances in Atmospheric Science and Applications', Heraklion, Greece, 8–12 June 2015 (ESA SP-735, November 2015)

Operation, MarcoPolo, project aims to procure up-to-date regional air pollution information and means for emission control of the main atmospheric. In the current work, the focus falls on SO_2 and especially emission estimates from space and the refinement of these emission estimates by spatial downscaling and by source sector apportionment. A wide range of data is used from various satellite instruments as described below. From these satellite data, emission estimates are expected to be made for anthropogenic and biogenic sources and with various state-of-the-art techniques, up-to-date emission inventories are to be created [9; 10]. By combining these emission data with known ground-based information a new emission database for MarcoPolo will be constructed. The new emission inventory is input to air quality models and is expected to improve the existing air quality modeling and forecasts considerably. In the following we demonstrate the capability of three different satellite instruments of discerning the anthropogenic SO_2 load over China as a first step towards the aforementioned goals.

2. DATA AND METHODOLOGY

2.1 Satellite SO_2 observations

Sulphur dioxide columns from the SCIAMACHY/Envisat, GOME2/MetopA and OMI/Aura sensors have been obtained and analyzed in order to study the spatiotemporal evolution of the total SO_2 load over the greater China area from year 2004 to 2014 inclusive depending on the time span of each satellite instrument. In the following, a short description of both instruments and algorithms is given.

2.1.1 GOME2/MetopA

The Global Ozone Monitoring Experiment-2 (GOME-2) instrument was launched onboard the EUMETSAT MetOp-A satellite in October 2006. MetOp-A is flying on a sun-synchronous orbit with an equator crossing time of 09:30 local time (descending node) and a repeat cycle of 29 days. GOME-2 is a nadir-scanning UV-VIS spectrometer with four main optical channels, covering the spectral range between 240 and 790 nm with a spectral resolution between 0.26 nm and 0.51 nm. The default swath width of the GOME-2 scan is 1920 km, which enables global coverage in about 1.5 days with a default ground footprint size of 80×40 km^2 [11].

The operational off-line GOME-2 total SO_2 columns from MetOp-A are generated at the German Aerospace Center (DLR) using the Universal Processor for UV/VIS Atmospheric Spectrometers environment version 1.3.9, implementing the level-1-to-2 GDP 4.7 algorithm. The data processing is commissioned by EUMETSAT within the auspices of the Satelite Application Facility for Atmospheric Composition and UV Radiation, O3MAF project [12]. The GOME Data Processor (GDP) is the operational algorithm for the retrieval of trace gas columns including total SO_2 from GOME-2. GDP 4.7 is the latest incarnation of the GDP 4 algorithm [13;14] which employs the two step Differential Optical Absorption Spectroscopy (DOAS) method, with slant column fitting followed by Air Mass Factor (AMF) conversion to the vertical column density (VCD) [15]. Further information on the validation of the GDP4.7 total SO_2 columns can be found in the official Validation Report [16] found here: This GOME2/MetopA dataset was downloaded from http://atmos.eoc.dlr.de/gome2/.

A slightly different version of the GOME-2 total SO_2 columns from MetOp-A are extracted at the Support to Aviation Control Service (SACS) service hosted by the Belgian Institute for Space Aeronomy (BIRA) which aims at supporting the Volcanic Ash Advisory Centers, like Toulouse VAAC and London VAAC [17]. This version is based on the near-real-time, NRT, operational GOME-2 total SO_2 columns from MetOp-A generated at DLR for EUMETSAT. More information on the NRT algorithm can be found in the Algorithm Theoretical Basis Document [15]. This GOME2/MetopA dataset was downloaded from the site of the SACS service at http://sacs.aeronomie.be/.

2.1.2 SCIAMACHY/Envisat

The Scanning Imaging Absorption spectroMeter for Atmospheric CartograpHY (SCIAMACHY) was launched in March 2002 aboard the European platform ENVISAT and has been operational for more than ten years providing global coverage in approximately six days [18]. ENVISAT was in a Sun-synchronous orbit with an inclination of 98.5°, a mean altitude of 796 km and has a period of 100 min, performing about 14 to 15 orbits per day. SCIAMACHY is an eight-channel spectrometer covering the spectral range from 240 nm to 2380 nm and uses different viewing geometries for retrieving total trace gas columns (nadir) and profiles (limb and solar/lunar occultation). The nominal swath is 960 km with a typical footprint size of 60 km x 30 km for ozone observations, global coverage is achieved at the equator within six days.

The operational SCIAMACHY/Envisat total SO_2 column data used in this study are retrieved with the SGP 5.02 processor [19] and are distributed as SCIAMACHY total column densities and stratospheric profiles of various trace gases from the ESA Earth OnLine site at https://earth.esa.int.

A different version of the SCIAMACHY/Envisat total SO_2 columns are generated at the SACS service hosted by BIRA. Details on this product can be found in [17;20] as well as in the Algorithm Theoretical Basis Document, [21] and the Product Validation Document [22]. This SCIAMACHY/Envisat dataset was downloaded from http://sacs.aeronomie.be/.

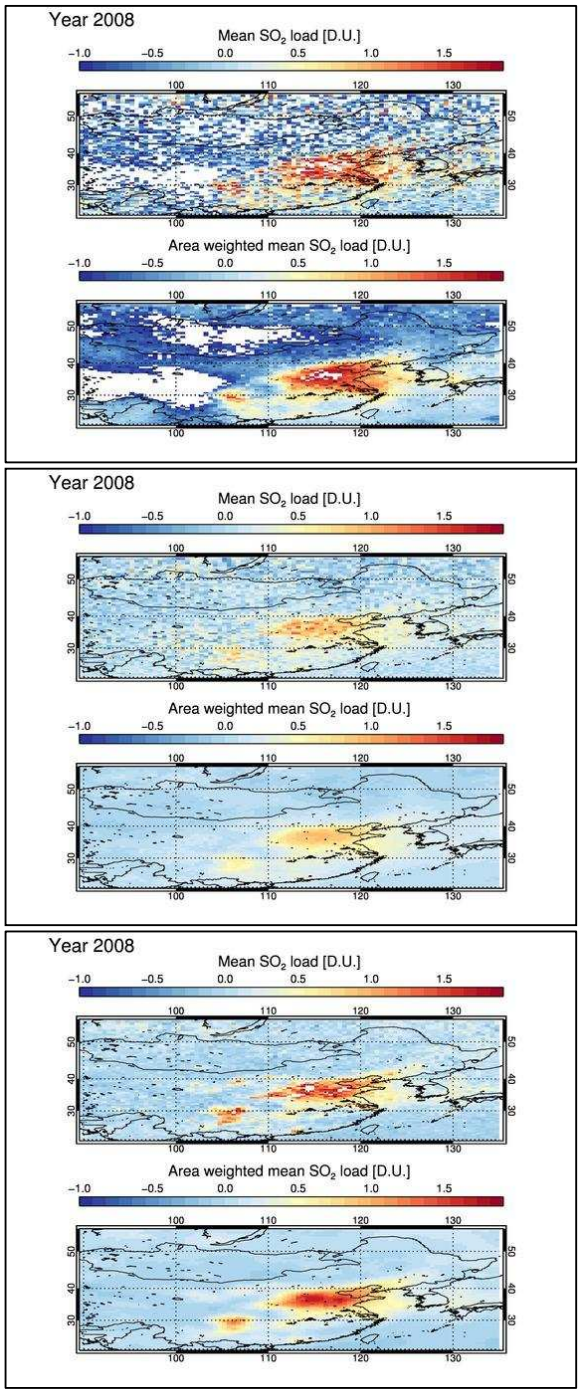

Figure 1. The yearly SO_2 loading over East Asia, centered over China, as seen by SCIAMACHY/Envisat [top], GOME2/MetopA [middle] and OMI/Aura [bottom] for year 2008. The official algorithms by ESA [top], EUMETSAT [middle] and NASA [bottom] are shown. The data have been gridded in 0.5x0.5° bins. The upper plot shows SO_2 averages within the grid bin, whereas the bottom plot shows averages including the eight surrounding cells.

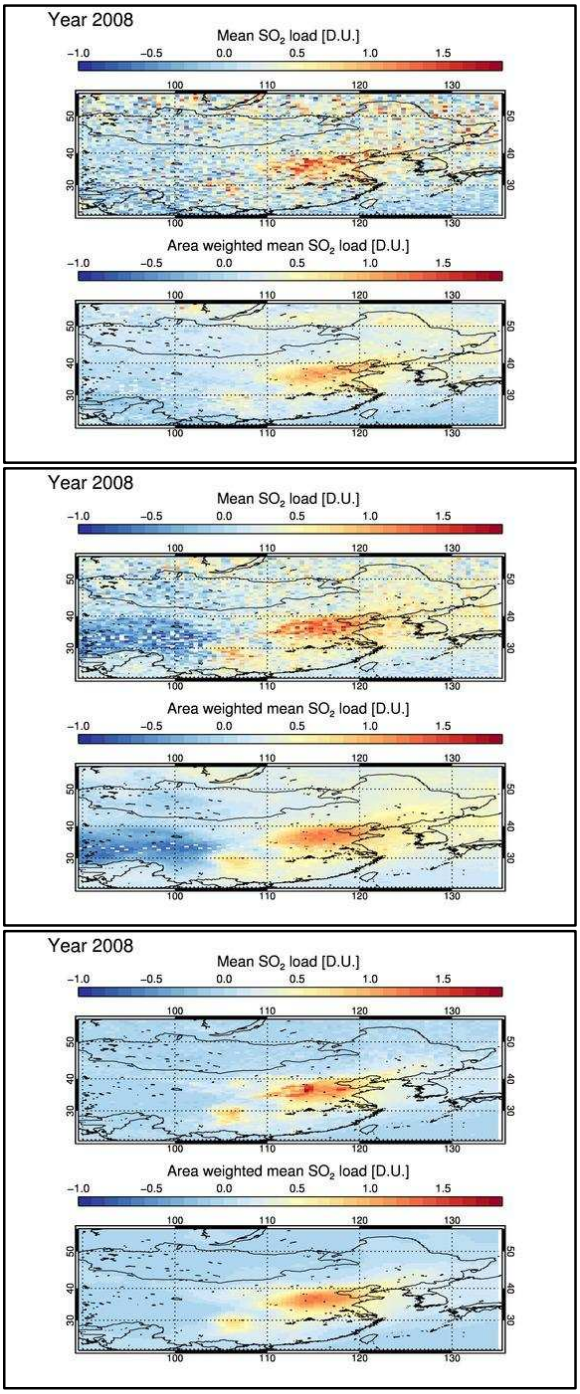

Figure 2. The yearly SO_2 loading over East Asia, centered over China, as seen by SCIAMACHY/Envisat [top], GOME2/MetopA [middle] and OMI/Aura [bottom] for year 2008. The BIRA algorithm [top], EUMETSAT [middle] and BIRA [bottom] are shown. The data have been gridded in 0.5x0.5° bins. The upper plot shows SO_2 averages within the grid bin, whereas the bottom plot shows averages including the eight surrounding cells

2.1.3 OMI/Aura

The Ozone Monitoring Instrument (OMI) is a Dutch/Finnish instrument flying on the AURA satellite of NASA launched in July 2004 on a sun-synchronous polar orbit with a period of 100 min and an Equator crossing time of about 13:45 LT on the ascending node. OMI is a nadir-viewing imaging spectrograph that measures atmosphere-backscattered sunlight in the ultraviolet-visible range from 270 to 500 nm with a spectral resolution of about 0.5 nm [23]. In contrast to GOME-2, operating with a scanning mirror and one dimensional photo diode array detectors, OMI is equipped with two-dimensional charge-coupled device (CCD) detectors, recording the complete 270–500 nm spectrum in one direction, and observing the Earth's atmosphere with a 114° field of view, distributed over 60 discrete viewing angles, perpendicular to the flight direction. The field of view of OMI corresponds to a 2600 km wide spatial swath completing global coverage within one day. Depending on the position across the track, the size of an OMI pixel varies from 13 km×24 km at nadir to 13 km×128 km for the extreme viewing angles at the edges of the swath. It should be stressed that due to a blockage affecting the nadir viewing port of the sensor, the radiance data of OMI are altered at all wavelengths for some particular viewing directions of OMI. This row anomaly (changing over time) can affect the quality of the products and hence reduce the spatial coverage of the data [24].

The operational OMI total SO_2 columns from AURA are generated and distributed by NASA [25]. The OMI planetary boundary layer [PBL] SO_2 data are now produced with a completely different retrieval algorithm based on principal component analysis [PCA] of the OMI radiance data [26]. Previously the OMI PBL SO2 data were produced using the Band Residual Difference [BRD] algorithm [27]. While the BRD algorithm is sensitive to SO_2 pollution in the PBL, it tends to have large noise and unphysical biases particularly at high latitudes. The PCA algorithm has greatly improved the quality of OMI SO_2 retrievals and has been implemented for operational production of the next generation OMI standard SO_2 product. This dataset was downloaded from http://avdc.gsfc.nasa.gov.

A new version of the OMI/Aura total SO_2 columns have been very recently presented in [28].The retrieval scheme includes a DOAS spectral fitting, a background correction, and the calculation of air mass factors and vertical column averaging kernels. Fixed UTLS SO_2 profiles are used as input to the algorithm for volcanic SO_2 plumes and simulations from the global chemical transport model IMAGES to represent SO_2 profiles for anthropogenic emissions. In the same paper, preliminary comparisons to OMI/Aura columns retrieved from the PCA algorithm discussed above over Eastern U.S. and Eastern China are shown. The results from the two algorithms are in good agreement overall with have very good and comparable SO_2 detection limits of around 0.5–0.6 D.U.

2.2 Analysis and methodology

For all algorithms discussed above, daily total SO_2 measurements reported for the PBL layer which depict the anthropogenic contribution for the atmospheric SO_2 load [as is defined by each methodology] where extracted for the period January 2004 to December 2014 inclusive where applicable. The domain chosen spans from 90° to 135° E and from 20° to 55° N. A common processing for all satellites & algorithms was enforced with the following restrictions: solar zenigth angle less than 70°, cloud fraction less than 20% and a maximum value for the reported VCD of less than 15 D.U. so as to avoid possibility of volcanic influence in the daily measurements. From the daily fields, monthly mean fields were created using a grid of 0.25°x0.25° in latitude and longitude and similarly yearly fields. Further to the whole domain, the loading at selected locations including 115 power plants and 35 cities was analysed All SO_2 measurements falling within three radii [20km, 40km & 60 km] are assigned to the grid cell, creating three different time series for the ground source.

3. RESULTS

In Figure 1 and Figure 2 the mean annual SO_2 loading for year 2008 is presented for all satellite instruments and algorithms as first view of the datasets. The methodology has been described in Section 2.2, with the only variation being that the grid onto which the data have been averaged is slightly larger, 0.5°x0.5° [for viewing purposes]. In both Figures the SCIAMACHY/Envisat observations are shown at the top, the GOME2/MetopA in the middle and the OMI/Aura at the bottom panels. The upper plot shows SO_2 averages only within the grid cell, whereas the bottom plot shows averages including the eight surrounding cells. In Figure 1 the official algorithms by ESA [top], EUMETSAT [middle] and NASA [bottom] are given whereas in Figure 2 the BIRA algorithm [top], EUMETSAT [middle] and BIRA [bottom] are shown. The same color scale was used in all cases for easy comparison. A first point to note is that for the instruments with larger footprint, namely SCIAMACHY [top] and GOME2 [middle], averaging the data including the surrounding cells does improve the noise of the dataset, already visually. For OMI [bottom], with the smallest footprint, the two methods appear near identical. The SCIAMACHY coverage, due to its sparser temporal coverage, appears nosier. The known China hotspots are well revealed in all cases.

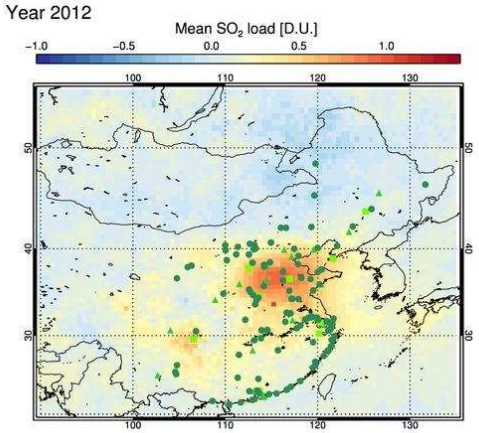

Figure 3. Location of known point sources of SO_2 around China. The different symbols denote cities [green triangle], as well as small emitting plants[green circles], medium [light green squares] and strong [dark green squares] emitting power plants.

In order to investigate in detail the behavior of the satellite estimates over known hotspots, the locations of 115 power plants and 35 megacities have been identified and further analysis was performed on them. In Figure 3 these locations are shown against a backdrop of the SO_2 loading seen by GOME2/MetopA for year 2012. The separation of the emitting load of the power plants was performed *ad hoc*, characterizing "small plants" as those emitting up to 2200MW, "medium plants" those emitting between 2200 and 3500 MW and "strong plants " those emitting above 3500 MW. From the map it is obvious that even though some locations are covered, there exist hot-spots not included in our list, such as the coal mining activities around 105°E and 30°N among others. The locations list is hence under constant update and investigation.

Focusing on some of the more interesting hotspots, in Figure 4 and Figure 5 the time series for three locations are given. The format of these Figures follows those of Figure 1 and Figure 2. For all cases, three different averaging choices were explored: in red, the gridding was performed within 20km of the point source; in blue within 40km and in green within 60km. The trend in D.U. per annum is also shown in the upper right corner of each graph. In the upper row of Figure 4 and Figure 5, for the SCIAMACHY algorithms, the time series for the city of Shanghai, the largest city in China with an estimated population of 35 million, is shown. Of note are the high inter-annual scatter bars showing the high variability of the SCIAMACHY product, not least caused by the low representativeness of the measurements due to the six day coverage. The highly negative trend found for the SCIAMACHY/ESA dataset [upper, Figure 4] of -0.12 D.U./annum is not statistically significant, however the lower one found by SCIAMACHY/BIRA [upper, Figure 5] of -0.05 D.U./annum is associated with a significance level of 94% [from an original two-sided 0.05 percentile]. In the middle panel of the same Figures, the GOME2 time series for Lingwu, the most important industrial city of the Ningxia Hui Autonomous Region, in the northwestern region of the People's Republic of China, is shown. Even though the winter months are under-represented in the monthly means, due to the strict restriction on the SZA values permitted, a positive trend [*albeit* non-significant] is reported by both the OTO and the NRT GOME2/EUMESAT data. The large monthly mean values observed in autumn and spring of 2011 are under investigation. Finally, in the bottom panel of Figure 4 and Figure 5, the time series of the SO_2 loading for the city of Shijiazhuang which is the capital and largest city of North China's Hebei Province are given. At the 2010 census, it had a total population of more than 10 million people and from 2008 to 2011, Shijiazhuang implemented a three-year plan which concluded with the reorganization of the city resulting in an increase of green areas and improved urbanization (new buildings, new roads and road plans). It might not hence come as a surprise that both negative trends reported by the two OMI/Aura algorithms are statistically significant to more than 99%, depicting this turn towards greener energy and clean air for the region.

4. CONCLUSIONS & FURTHER WORK

Within the auspices of the EU FP7 *Monitoring and Assessment of Regional air quality in China using space Observations, Project Of Long-term sino-european co-Operation*, MarcoPolo, project, we have presented long term satellite observations of Sulphur Dioxide, SO_2, over the greater China area. Observations from the SCIAMACHY/Envisat, GOME2/MetopA and OMI/Aura instruments have been analysed using the same methodologies and tools and their relative strong points and limitations have been discussed. Close to 150 locations of specific interest around the region were examined in detail and their trends in time assessed. Even though a number of locations with a positive SO_2 trend have been identified, the significant ones apply to negative trends with roughly half the power plant locations and one third of the populated areas following that pattern. In the future, with the aid of a local SO_2 bottom-up emission inventory, the variability of SO_2 at these locations will be further investigated and the possibility of using these satellite measurements as input for a top-down emission inventory will be assessed.

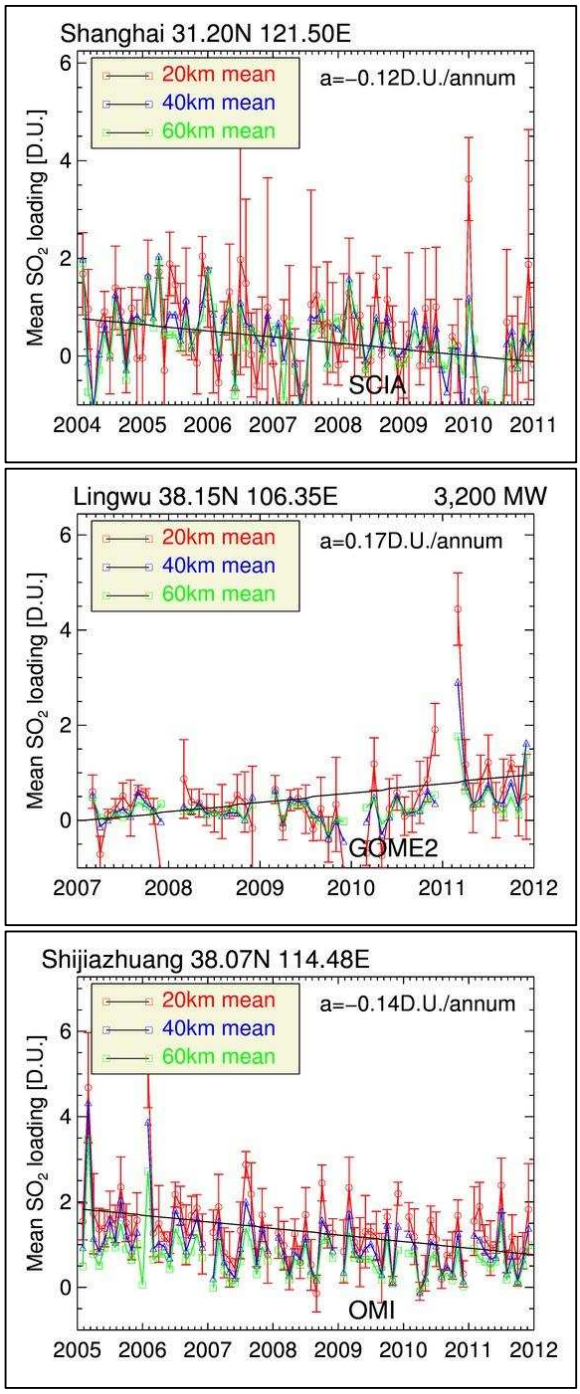

Figure 4.Time series of the SO_2 loading three selected regions discussed in the text. SCIAMACHY/Envisat [top], GOME2/MetopA [middle] and OMI/Aura [bottom] The official algorithms by ESA [top], EUMETSAT [middle] and NASA [bottom] are shown. The different colored line show the distance of averaging from the central point. The trend per annum is also given on the top right.

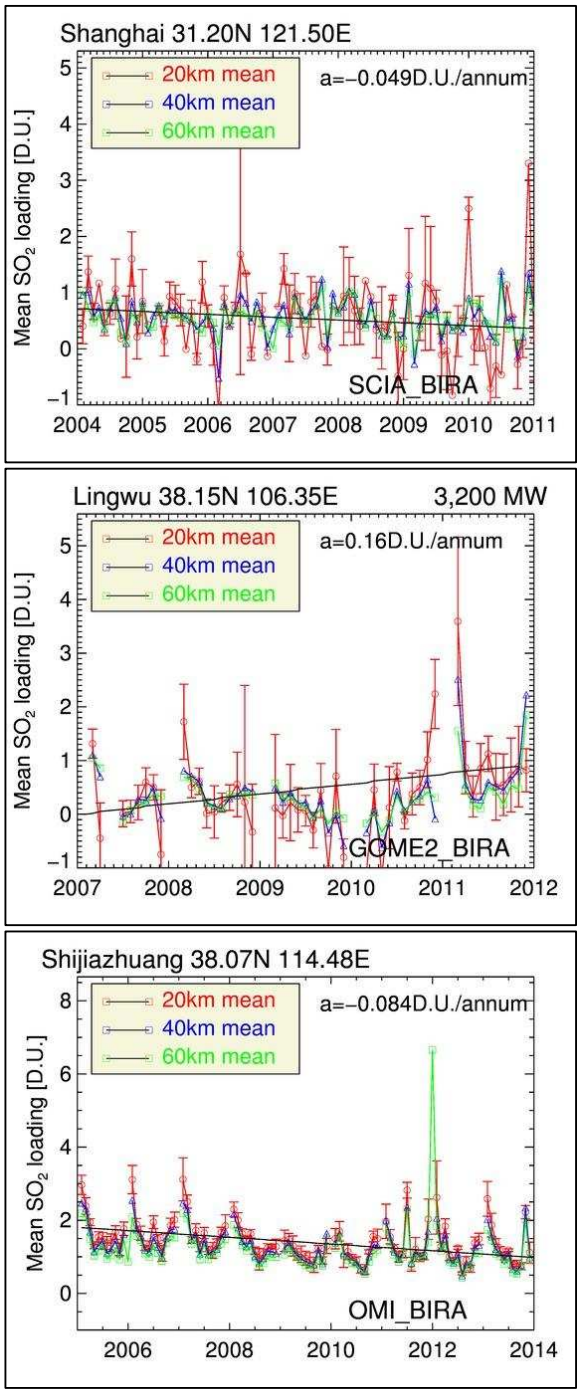

Figure 5. Time series of the SO_2 loading three selected regions discussed in the text. SCIAMACHY/Envisat [top], GOME2/MetopA [middle] and OMI/Aura [bottom]. The BIRA algorithm [top], EUMETSAT [middle] and BIRA [bottom] are shown. The different colored line show the distance of averaging from the central point. The trend per annum is also given on the top right.

5. REFERENCES

1. Damoah, R., et al., (2004), Around the world in 17 days - hemispheric-scale transport of forest fire smoke from Russia in May 2003, *Atmos. Chem. Phys.*, 4, 1311-1321, doi:10.5194/acp-4-1311-2004.
2. Dirksen, R. J.,et al., (2009), An aerosol boomerang: Rapid around-the-world transport of smoke from the December 2006 Australian forest fires observed from space, *J. Geophys. Res.*, 114, D21201, doi:10.1029/2009JD012360.
3. Benkovitz, C. M., et al., (2004), Modeling atmospheric sulfur over the Northern Hemisphere during the Aerosol Characterization Experiment 2 experimental period, *J. Geophys. Res.*, 109, D22207, doi:10.1029/2004JD004939.
4. Streets, D. G., et al. (2003), An inventory of gaseous and primary aerosol emissions in Asia in the year 2000, *J. Geophys. Res.*, 108(D21), 8809, doi:10.1029/2002JD003093.
5. He, H., et al. (2012), SO_2 over central China: Measurements, numerical simulations and the tropospheric sulfur budget, *J. Geophys. Res.*, 117, D00K37, doi:10.1029/2011JD016473.
6. Krotkov, N. A., et al. (2008), Validation of SO_2 retrievals from the Ozone Monitoring Instrument over NE China, *J. Geophys. Res*., 113, D16S40, doi:10.1029/2007JD008818.
7. Li, C., et al., (2010), Recent large reduction in sulfur dioxide emissions from Chinese power plants observed by the Ozone Monitoring Instrument, *Geophys. Res. Lett.*, 37, L08807, doi:10.1029/2010GL042594.
8. Li, C., et al., (2010), Transport and evolution of a pollution plume from northern China: A satellite-based case study, *J. Geophys. Res.*, 115, D00K03, doi:10.1029/2009JD012245.
9. Fioletov, V. E., et al. (2011), Estimation of SO2 emissions using OMI retrievals, *Geophys. Res. Lett.*, doi:10.1029/2011GL049402.
10. Fioletov, V. E., et al. (2013), Application of OMI, SCIAMACHY, and GOME-2 satellite SO2 retrievals for detection of large emission sources, *J. Geophys. Res.*, doi:10.1002/jgrd.50826.
11. Munro, R., et al., (2006), GOME-2 on MetOp, in: *Proc. of the 2006 EUMETSAT Meteorological Satellite Conference*, Helsinki, Finland, p. 48, EUMETSAT.
12. http://o3msaf.fmi.fi/projectinfo.html, last accessed: 03 June 2015.
13. Van Roozendael M., et al., (2006), Ten years of GOME/ERS-2 total ozone data—The new GOME data processor (GDP) version 4: 1. Algorithm description, *J. Geophys. Res.*, 111, D14311, doi:10.1029/2005JD006375.
14. Loyola, D. G., et al., (2011), The GOME-2 total column ozone product: Retrieval algorithm and ground-based validation, *J. Geophys. Res.*, 116, D07302, doi:10.1029/2010JD014675.
15. http://o3msaf.fmi.fi/docs/atbd/Algorithm_Theoretical_Basis_Document_NTO_OTO_May_2013.pdf , last accessed: 03 June 2015.
16. http://o3msaf.fmi.fi/docs/vr/Validation_Report_OTO_SO2_Jun_2013.pdf, last accessed: 03 June 2015.
17. Brenot et al., (2014), Support to Aviation Control Service (SACS): an online service for near real-time satellite monitoring of volcanic plumes, *Natural Hazards and Earth System Sciences*.
18. Bovensmann, H., et al., (1999), SCIAMACHY: Mission objectives and measurement modes, *J. Atmos. Sci.*, 56, 2, 127–150.
19. https://earth.esa.int/handbooks/availability/disclaimers/SCI_OL__2P_README.pdf, last accessed: 03 June 2015.
20. Theys et al., (2013), Volcanic SO_2 fluxes derived from satellite data: a survey using OMI, GOME-2, IASI and MODIS, *Atmos. Chem. Phys.*, 13, 5945-5968, doi:10.5194/acp-13-5945-2013.
21. http://sacs.aeronomie.be/Documentation/SACSplus_ATBD.pdf, last accessed: 03 June 2015.
22. http://sacs.aeronomie.be/Documentation/SACSplus_PVD.pdf, last accessed: 03 June 2015.
23. Levelt P.F., et al., (2006), The Ozone Monitoring Instrument, *IEEE Trans. Geosc. Rem. Sens.*, 44 (5), 1093-1101.
24. http://www.knmi.nl/omi/research/product/rowanomaly-background.php, last accessed: 03 June 2015.
25. http://disc.sci.gsfc.nasa.gov/Aura/data-holdings/OMI/omno2g_v003.shtml, last accessed: 03 June 2015.
26. Li et al., (2013), A fast and sensitive new satellite SO_2 retrieval algorithm based on principal component analysis: Application to the ozone monitoring instrument, *Geophys. Res. Let.*, 40, 6314–6318, doi:10.1002/2013GL058134.
27. Krotkov et al., (2006), Band residual difference algorithm for retrieval of SO_2 from the Aura Ozone Monitoring Instrument (OMI), *IEEE Trans. Geosci. Remote Sensing*, doi: 10.1109/TGRS.2005.861932.
28. Theys, N., I. et al., (2015), Sulfur dioxide vertical column DOAS retrievals from the Ozone Monitoring Instrument: Global observations and comparison to ground-based and satellite data, *J. Geophys. Res. Atmos.*, 120, 2470–2491. doi: 10.1002/2014JD022657.

6. ACKNOWLEDGMENETS

Results presented in this work have been produced using the European Grid Infrastructure (EGI) through the National Grid Infrastructures NGI_GRNET (HellasGrid) as part of the SEE Virtual Organization. The authors would like to acknowledge the support provided by the Scientific Computing Office, IT A.U.Th. throughout the progress of this research work.